Received: 14 September 2021 | Revised: 8 March 2022 | Accepted: 16 March 2022

DOI: 10.1002/jsp2.1198

RESEARCH ARTICLE

JOR Spine OPEN ACCESS

Comparison and optimization of sheep in vivo intervertebral disc injury model

Caroline Constant[1] | Warren W. Hom[2] | Dirk Nehrbass[1] | Eric-Norman Carmel[3] | Christoph E. Albers[4] | Moritz C. Deml[4] | Dominic Gehweiler[1] | Yunsoo Lee[2] | Andrew Hecht[2] | Sibylle Grad[1] | James C. Iatridis[2] | Stephan Zeiter[1]

[1]AO Research Institute Davos, Davos, Switzerland

[2]Department of Orthopaedics, Icahn School of Medicine, Mount Sinai Health System, New York, New York, USA

[3]Département de sciences cliniques, Faculté de médecine vétérinaire, Université de Montréal, Saint-Hyacinthe, Canada

[4]Department of Orthopaedic Surgery & Traumatology, Inselspital, University Hospital Bern, Bern, Switzerland

Correspondence
Caroline Constant, AO Research Institute Davos, Clavadelerstrasse 8, CH 7270, Davos, Switzerland.
Email: caroline.constant@aofoundation.org

Funding information
This work was supported by the National Institute of Arthritis and Musculoskeletal and Skin Diseases [NIH R01 AR057397], the AO Foundation, and AO Spine.

Abstract

Background: The current standard of care for intervertebral disc (IVD) herniation, surgical discectomy, does not repair annulus fibrosus (AF) defects, which is partly due to the lack of effective methods to do so and is why new repair strategies are widely investigated and tested preclinically. There is a need to develop a standardized IVD injury model in large animals to enable comparison and interpretation across preclinical study results. The purpose of this study was to compare *in vivo* IVD injury models in sheep to determine which annulus fibrosus (AF) defect type combined with partial nucleus pulposus (NP) removal would better mimic degenerative human spinal pathologies.

Methods: Six skeletally mature sheep were randomly assigned to one of the two observation periods (1 and 3 months) and underwent creation of 3 different AF defect types (slit, cruciate, and box-cut AF defects) in conjunction with 0.1 g NP removal in three lumbar levels using a lateral retroperitoneal surgical approach. The spine was monitored by clinical CT scans pre- and postoperatively, at 2 weeks and euthanasia, and by magnetic resonance imaging (MRI) and histology after euthanasia to determine the severity of degeneration (disc height loss, Pfirrmann grading, semi-quantitative histopathology grading).

Results: All AF defects led to significant degenerative changes detectable on CT and MR images, produced bulging of disc tissue without disc herniation and led to degenerative and inflammatory histopathological changes. However, AF defects were not equal in terms of disc height loss at 3 months postoperatively; the cruciate and box-cut AF defects showed significantly decreased disc height compared to their preoperative height, with the box-cut defect creating the greatest disc height loss, while the slit AF defect showed restoration of normal preoperative disc height.

Conclusions: The tested IVD injury models do not all generate comparable disc degeneration but can be considered suitable IVD injury models to investigate new treatments. Results of the current study clearly indicate that slit AF defect should be

This is an open access article under the terms of the Creative Commons Attribution-NonCommercial-NoDerivs License, which permits use and distribution in any medium, provided the original work is properly cited, the use is non-commercial and no modifications or adaptations are made.
© 2022 The Authors. *JOR Spine* published by Wiley Periodicals LLC on behalf of Orthopaedic Research Society.

avoided if disc height is used as one of the main outcomes; additional confirmatory studies may be warranted to generalize this finding.

KEYWORDS
annulus fibrosus defect, discectomy, intervertebral disc degeneration, intervertebral disc injury, preclinical model, sheep

1 | INTRODUCTION

Back pain is the most common musculoskeletal complaint, with a prevalence of up to 30% in the general population.[1] Unfortunately, this pain becomes chronic in 7%–10% of patients.[2] Intervertebral disc (IVD) degeneration is commonly accepted as one of the main causes of low back pain.[3] The pain resulting from alteration in IVD structure can partially be explained by the loss of its load-bearing function during bending and twisting movements.[4] Many alterations to the IVD occur during disc degeneration, with disc herniation (prolapse) being the most common source of pain and disability.[3,5] The herniation of the nucleus pulposus (NP) becomes possible with the accumulation of micro-fissures and tearing in the annulus fibrosus (AF) secondary to disorganization of its lamellar collagen fiber network.[4,6] Degeneration of the IVD and its treatment are intensely researched to improve the substantial morbidity and disability associated with the condition. Some studies suggest discectomy procedures without additional treatments as the standard of care for herniation with improved outcomes compared to nonoperative treatment.[7,8] Nevertheless, a complication occurs in up to 25% of patients, and reherniation and recurrent back pain at the same level are frequently encountered postoperatively.[9,10] To improve surgical outcomes after discectomy procedures, new strategies based on biomaterial and tissue engineering are under investigation.

The efficacy investigation of new repair strategies targeting the AF and/or NP after the discectomy procedure often requires preclinical testing prior to clinical application. For this purpose, many different in vivo models have been described in small and large animals.[11–24] The choice of animal models will influence the type and severity of IVD injury required to induce degeneration. Indeed, animal species particularities such as disc height, notochordal cells, and NP fibrosity influence the IVD response to injury and subsequent degeneration.[25–27] Sheep models are suitable for translation to human spinal pathology because of their similarities, including comparable vertebral body and endplate morphology, similar loads experienced by the spine, and resemblances in their IVD cellular content (Figure 1).[28–31] Sheep lumbar spine has been extensively used to evaluate the effect of adjuvant treatment of discectomy as it is considered to approximate the state of human IVD after discectomy.[32,33] Previous works on sheep described a multitude of IVD injury models (annulotomy and removal of NP) of various degrees of severity from a simple cut in the AF[14,34–36] to a drill-bit injury in all IVD structures.[33] The degree and consistency of IVD degeneration are not necessarily comparable between those described models. Osti et al.[14] were the first to describe a successful model of IVD injury leading to degeneration in sheep by partial-thickness incision of the AF. However, this model showed pathological changes across a 12- to 18- month period, which limits its possible use in preclinical research. Melrose et al.[16] described an optimized annular lesion of the anterolateral AF (20-mm wide and 6-mm deep) capable of reproducing disc height loss 3 months postoperatively. This model represented a good tool for investigating potential therapeutic interventions but failed to induce disc herniation. In general, aggressive AF defect creation (annulotomy) and NP removal are believed to produce more consistent IVD

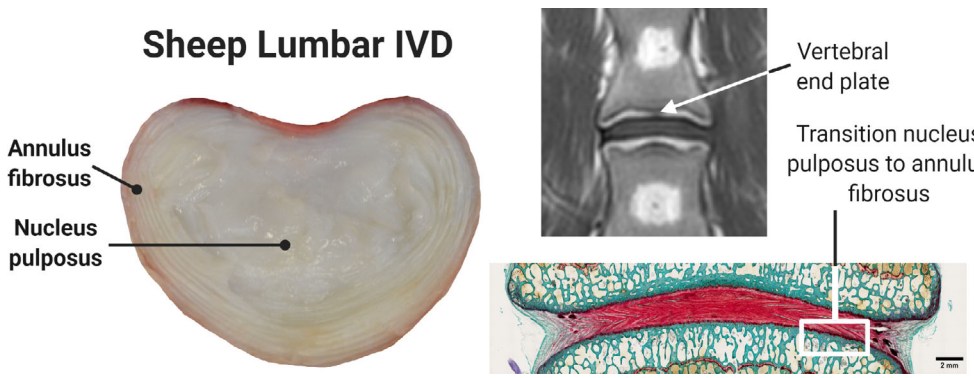

FIGURE 1 Sheep lumbar spine across multiple imaging modalities. Normal macroscopic intervertebral sheep disc anatomy in superior cross-sectional view (left). Magnetic resonance imaging (MRI) in T1 sequence, coronal view, showing the intervertebral disc (IVD) between the 2 adjacent end plates (top right). Histological Safranin O-stained image, dorsal view, showing the normal transition between the IVD tissues (bottom right)

degeneration in vivo.[26,32,33] However, there is no consensus on the most suitable and reliable large animal IVD injury model to investigate new treatment strategies following discectomy procedures and capable to mimic degenerative human spinal pathologies and disc herniation.[16,31]

There remains a growing need to characterize a standardized and robustly evaluated AF defect model in sheep since the variability within preclinical IVD injury models decreases the ability to compare the results between studies and could lead to misinterpretation of preclinical study results. To address these important shortcomings, this study compared sheep in vivo IVD injury models to determine the AF defect type (slit, cruciate, box-cut AF defect) combined with partial NP removal that would mimic degenerative human spinal pathologies and would induce the greatest amount of disc material herniation and short-term disc height loss. The hypothesis was that AF defect using a box-cut technique (annulectomy) would lead to a greater amount of disc herniation, increased disc height loss, and accelerated degenerative changes compared to slit and cruciate AF defects.

2 | MATERIAL AND METHODS

2.1 | Study design and preclinical model overview

Six skeletally mature female Swiss White Alpine sheep were enrolled in the study and randomly assigned to one of the two observation periods: 1 and 3 months (n = 3 sheep per period). Each sheep underwent the creation of 3 different AF defect types (slit, cruciate, box-cut AF defects) and standardized 0.1 g NP removal in three lumbar levels (L1-L2, L2-L3, L3-L4; type of AF defect with 0.1 g NP removal per

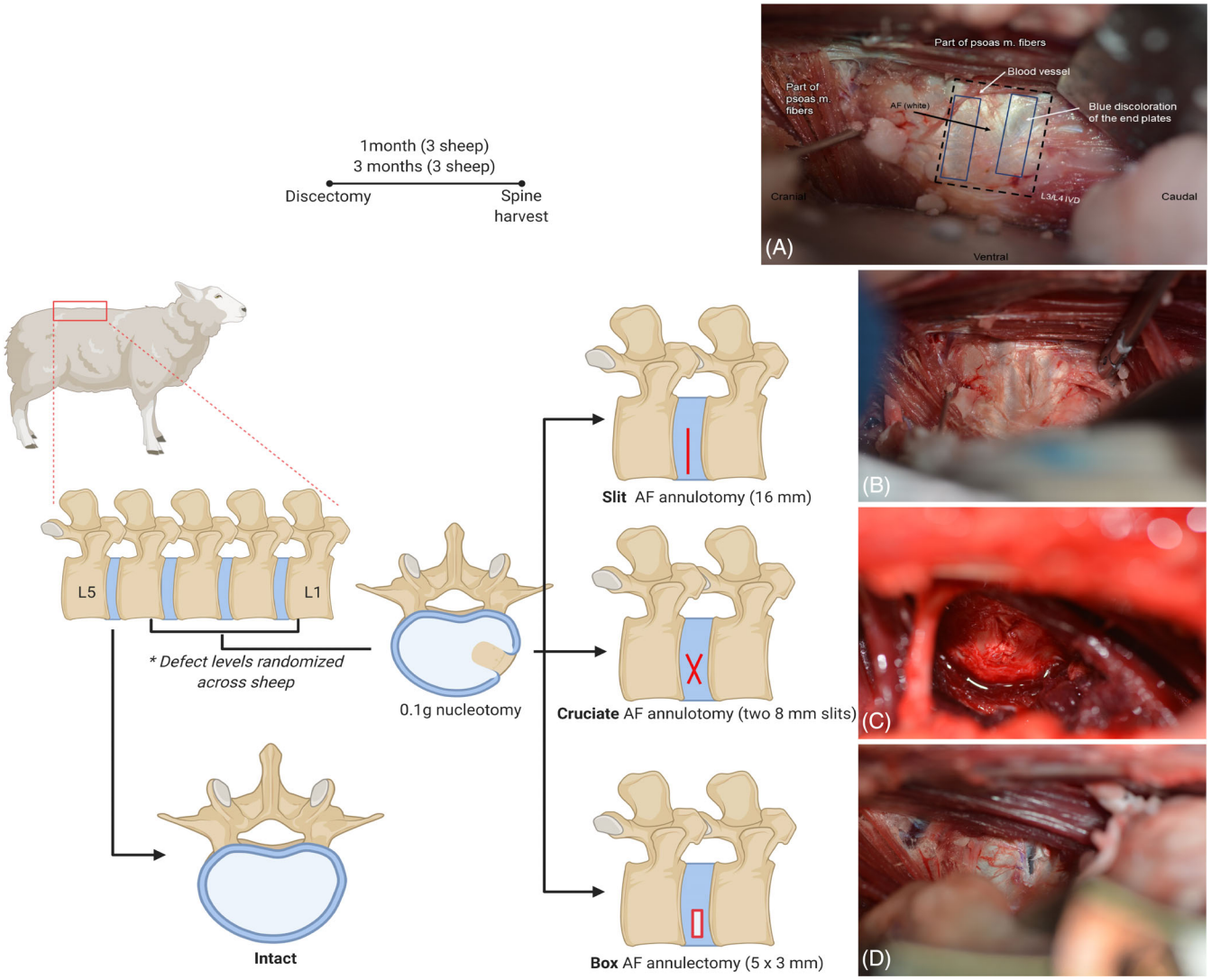

FIGURE 2 Study design of *in vivo* sheep lumbar spine model. Schematics and intraoperative images depicting the annulus fibrosus (AF) defects created in conjunction with nucleus pulposus removal. Intraoperative images are oriented with the cranial side of the sheep to the left, caudal to the right, ventral on the bottom, and dorsal on the top. The lumbar spine was visualized through a lateral retroperitoneal surgical approach and the intervertebral discs) were exposed (A), and those receiving the discectomy injury were subjected to a 16 mm AF annulotomy (B), two 8 mm AF annulotomies in a cruciate pattern (C), or a 5 mm by 3 mm box-cut annulectomy (D)

IVD) using a lateral retroperitoneal surgical approach. AF defect types were alternated systematically by level (L1-L4) between the sheep. Lumbar level L4-L5 was left intact and served as intact control IVD. Each AF defect type and intact L4-L5 IVD represented an experimental group, and therefore each animal included all groups (Figure 2). During the postoperative period, animal welfare and body weight were monitored, the lumbar spine was monitored by clinical computer tomography (CT) immediately after the surgery, at 2 weeks postoperatively, and at euthanasia (at 1 or 3 months according to the observation period). Postmortem analyses included magnetic resonance imaging (MRI) and histology. The main outcomes were the severity of degenerative changes observed by medical imaging (disc height loss, Pfirrmann grading) as well as qualitative and semiquantitative histopathologic examination.

2.2 | Animals

The study adhered to the ARRIVE reporting standard for research (see Data S1; ARRIVE guidelines). The study was compliant with the Directive 2010/63/EU, approved by relevant Swiss authorities (Cantonal authorities in Graubünden, Switzerland: Permission # 19/2019), and performed in a facility accredited by the Association for Assessment and Accreditation of Laboratory Animal Care International (AAALAC). Six skeletally mature female Swiss Alpine sheep (age range 2–5 years, weight range 64.5–78 kg) were enrolled in the study and randomly assigned to the 1 month or 3 months observation period (n = 3 sheep per period). Prior to the start of the study, the sheep were kept in groups under a 12 h dark/light cycle and fed with hay and mineral supplements. They were acclimatized for at least 2 weeks to adapt to the local conditions and the animal caretakers. Preoperatively, the sheep were required to be in good health based on a complete physical assessment performed by a veterinarian and a complete blood cell count and free of signs of degenerative lumbar disease based on preoperative lumbar spine radiographs. Postoperatively, the sheep were housed in groups of three under the same conditions as listed above. Animal welfare assessment was performed by clinical physical examination using a score sheet twice daily for the first 3 days postoperatively followed by daily evaluation for 4 additional days, and then once weekly in conjunction with complete physical examinations performed regularly by an experienced veterinarian. The sheep's weight was also monitored weekly.

2.3 | Surgical intervention

Prior to general anesthesia, the sheep were maintained off-feed for 48 h. The sheep were sedated with Detomidine (0.04 mg/kg intramuscular [IM]) before general anesthesia induction using an intravenous mixture of midazolam (0.2 mg/kg intravenous [IV]) and ketamine (4 mg/ kg IV). Afterward, the sheep were endotracheally intubated and maintained under general anesthesia using sevoflurane volatile liquid anesthetic (2%–4% V/V in 0.5 L/min oxygen and air). Analgesia was provided preoperatively by nonsteroidal anti-inflammatory drug (Carprofen, 1.4 mg/kg IV) and lumbosacral epidural analgesia with buprenorphine (0.005 mg/kg added to 0.9% saline for a total 10 mL volume). Postoperative analgesia consisted of repeated nonsteroidal anti-inflammatory treatments for 5 additional days (carprofen, 4 mg/kg subcutaneous every 48 h), buprenorphine (0.05 mg/kg IM at the end of the surgical procedure, and every 6–8 h for 12–18 h) and transdermal fentanyl (2 μg/kg/h transdermal patch for 72 h, applied at the time of surgery). Antibiotic prophylaxis regimen included perioperative sodium-ceftiofur (2.2 mg/kg IV preoperatively and repeated every 90 min) followed by long-acting ceftiofur administered at the end of surgery (6.6 mg/kg IM).

For the surgical procedure, the sheep were placed in right lateral recumbency with the body slightly tilted ventrally and sandbags placed under the right side of the spine to assure straight alignment of the dorsal lumbar vertebral processes. After surgical aseptic skin preparation, the lumbar levels were exposed through a lateral retroperitoneal surgical approach. A longitudinal skin incision was made along a line from the dorsal spinous process of T12 to the ventral aspect of the L4 and continued through the subcutaneous fat, lumbar fascia, and the second layer of fat overlying the longissimus dorsi and iliocostalis muscles. After identification of L1 transverse process (located medial to the dorsal curvature of the thirteenth rib) using manual palpation and fluoroscopic guidance, a 1.25-mm Steinmann Pin was inserted into the lateral cortex of L2 vertebral body and used as a marker for intraoperative fluoroscopic guidance and postoperative medical imaging examinations. The lateroventral aspect of the lumbar IVD was exposed after separation and retraction of the musculature attaching to the dorsal aspect of each transverse process and ventral retraction of the psoas muscle using a SynFrame self-holding retractor (SynFrame RL, DePuy Synthes). Once the relevant IVD was identified and position confirmed by fluoroscopy, the loose fascia covering the ventrolateral AF was elevated and reflected cranially, preserving the blood vessels and nerves in the immediate area.

An AF defect (slit, cruciate, or box-cut, see below) was created prior to NP removal in the ventrolateral AF, not extending above the transverse process-vertebral body junction to avoid invasion of the spinal canal and damage to the spinal cord. Each AF defect was created in the predetermined lumbar level that was systematically rotated between the sheep. During AF defect creation, the depth of the scalpel stab was controlled at exactly 8 mm by using the end of the scalpel blade attachment to the scalpel blade holder as a stopper, resulting in uniform 8 mm depth and 0.4 mm thickness full-thickness annulotomy. The slit AF defect (full-thickness annulotomy) was created by a longitudinal cut in the lateral AF using a scalpel blade No. 11 and extended ventrally for a total length of 16-mm and 8-mm depth (Figure 2B). The cruciate AF defect (full-thickness annulotomy) was created by two cuts at 45° from the longitudinal IVD axis in the ventrolateral AF using a scalpel blade a No. 11 to span 8-mm width and 8-mm depth (Figure 2C). The box-cut AF defect (full-thickness annulectomy) resulted from the creation of 4 cuts of 8-mm depth to form a 5-mm length and 3-mm wide rectangular window in the

ventrolateral AF using a scalpel blade No. 11. The excised portion of the AF was removed prior to NP removal (Figure 2D).

After the creation of each AF defect, the nucleus was fenestrated, and 0.1 g of NP material was removed using Beck rongeurs (2-mm wide, 5-mm length). To ensure uniform partial discectomy, the NP was removed progressively and weighted with a high precision scale (+/− 0.001 g) until 0.1 g of NP was retrieved. Afterward, the NP was kept for histological analysis to determine if the vertebral endplates sustained iatrogenic trauma during the surgical procedure (see Histological Analysis). The AF defects were not sutured.

The surgical incision was closed with multiple continuous sutures using USP 0 polyglactin 910 through the lumbar fascial layer to reconstruct the muscle layers. The subcutaneous tissue was closed with a simple continuous suture using USP 2–0 poliglecaprone 25 and the skin with an intradermal suture using USP 3–0 poliglecaprone 25. An abdominal bandage was applied to cover the wound for the first week postoperatively with regular bandage changes.

2.4 | In vivo clinical CT

In vivo CT scans (Revolution EVO, GE Medical Systems, Switzerland) of the lumbar spine (L1 to L5) were acquired for all sheep pre- and post-IVD injury creation surgery, at 2 weeks postoperatively and at euthanasia (at 1 or 3 months according to the observation period) to determine disc height loss and degenerative changes over time. The scans were performed under general anesthesia with a standardized sheep position in dorsal recumbency with the hind limbs extended. The CT images were obtained with a slice thickness and spacing of 0.625 and 0.312 mm, respectively, using a tube voltage of 120kVp and tube current of 300 mA. The surgically placed Steinmann Pin through the lateral cortex of L2 served as an anatomical landmark to confirm the location of the studied IVD. CT images were evaluated by a blinded experienced board-certified veterinary surgeon (CC) for degenerative changes and a blinded observer (DG) for disc height calculation. Degenerative changes were assessed for each IVD based on the appearance of vertebral bones with particular attention to roughening of bone edges, presence, and severity of osteophytes or new bone formation bridging the IVD space. Disc height was measured using Amira software (Amira 6.5, FEI SAS a part of Thermo Fisher Scientific). To obtain the total disc height without the influence of variation in vertebral posture from sheep positioning, the lumbar vertebrae from the preoperative CT were semiautomatically segmented, separated, and the surface triangulated. From the obtained surfaces, the adjacent cranial and caudal IVD extremities (corresponding to the cranial and caudal vertebral endplates) were manually cut out. The distance between the resulting disc extremities (consisting of a surface mapped with approximately 4000 to 5000 points, depending on their sizes) was used to determine total disc height as follows. The distance from each point obtained at the cranial IVD extremity to the nearest point at the caudal IVD extremity was measured, and the arithmetic mean over all distances (corresponding to the height of the IVD at every single point) was calculated. The separated lumbar vertebrae and corresponding surfaces of IVD extremities obtained during the preoperative CT were rigidly registered and applied to their respective IVD extremities to determine the total disc height measurements postoperatively. The postoperative total disc height was then expressed in disc height variation as a percentage of respective preoperative disc height for each time point. Therefore, a disc height of less than 100% postoperatively would represent a disc height loss when compared to preoperative values.

2.5 | Euthanasia and sample harvest

The sheep were euthanized 1 month ($n = 3$ sheep) or 3 months ($n = 3$ sheep) after surgery according to their respective observation period by an overdose of pentobarbital (7.5 g IV), and the lumbar spine harvested. MRI images were acquired immediately after harvesting (see *Ex vivo* MRI). Subsequently, the individual IVD and adjacent vertebral endplates were bisected transversely using a butcher saw and fixed in 70% ethanol before further processing (see Histopathological analysis).

2.6 | *Ex vivo* MRI

MR images were acquired directly after lumbar spine harvesting with a 1.5 MRI scanner (Philips Medical Systems, Intera) using a sense-body imaging coil. The sequencing protocol used for IVD examination consisted of unenhanced axial, coronal, and sagittal T1- and T2-weighted sequences along with short tau inversion recovery (STIR). All MR images were reviewed by a blinded experienced board-certified veterinary radiologist (ENC) for comprehensive evaluation of lumbar disc degeneration according to predefined criteria (Table 1) with particular attention to presence or absence of annular fissure, end plate changes in signal intensity or morphology, in addition to presence and severity of changes in IVD height, IVD bulging, and IVD herniation.

Afterward, Pfirrmann disc degeneration grading scheme using axial and sagittal T2-weighted MR-images according to previously published work[38] (Figure 3) was performed by the same experienced observer (ENC) as well as 3 spine surgeons of different levels of experience who were trained before evaluating MR-images for this study: the observers were asked to strictly follow the Pfirrmann grading system provided as a handout along with a set of sample MRIs available to the observers during the image review. The observers were blinded to the sheep information, IVD status and observation period, and graded each of the 24 lumbar IVD (3 injured IVD and 1 intact control IVD per sheep; $n = 6$ sheep) independently and in random order. All IVD were analyzed twice by each observer on a separate occasion. To obtain a reference-grade for each IVD for further analysis, the mode Pfirrmann grade was used after all the data was collected.

TABLE 1 Parameters for magnetic resonance (MR) images evaluation

Parameters	Definition	Qualifications
IVD height	Qualitative assessment of the IVD height in comparison to control IVD (L4-L5)	Normal Decreased Collapsed
Annular fissure	Loss of the morphology of the AF characterized by separation between the annular fibers on T2 images representing fluid or granulation tissue.	Absent Present
End plate changes	Signs of degenerative or inflammatory changes involving the vertebral endplates characterized by change in signal intensity and/or morphology. Classified based on the location of the changes in regard to the endplates of the IVD being evaluated.	Absent Upper Lower Both
IVD bulging	Presence of disc tissue extending beyond the edges of the ring apophyses, throughout the circumference of the disc (not considered a form of herniation). When present, the bulging can be further classified as *diffuse*, if all the disc tissues are involved, or *asymmetric* when the disc tissue greater bulging is ≤50% of the disc circumference.	Absent Diffuse Asymmetric
IVD herniation	Defined as a focal displacement of disc material (≤ 25% of the disc circumference) beyond the limits of the intervertebral disc space. When present, the herniated disc can be further classified as *contained*, if the displaced portion is covered by outer annulus fibers and/or the posterior longitudinal ligament; or *uncontained* when there is no such covering.	Absent Contained Uncontained
IVD protrusion	With IVD herniation, Presence of herniation of nucleus material through the original defect or through another location in the annulus resulting in a focal "out-pouching" of the disc contour beyond the normal outer limits of the disc[37]	Absent Present
IVD extrusion	With IVD herniation, Presence of herniation of disc material through the original defect or through another location in the annulus such that disc material breaks through the confines of the annulus fibrosus[37]	Absent Present

Note: Parameters used for comprehensive MR-images evaluation of control and injured IVD.

2.7 | Histopathological analysis

Harvested lumbar segments were fixed in 70% ethanol, dehydrated, and embedded in methylmethacrylate. Afterward, dorsal sections (approximatively 300 μm wide) from the injured and control IVD were stained with Safranin-O/Fast Green for semiquantitative assessment of the degree of disc degeneration. The stained sections were graded by one blinded certified veterinary pathologist (DN) using a five-category grading scheme (grade 0–4) across six evaluated categories adapted from Shu et al. (Table 2).[39] The total histological score was calculated by summing grades across all categories: proteoglycan depletion, IVD structure and lesion morphology, cellular morphology, blood vessel ingrowth, cellular influx into the lesion, and cleft formation. In addition, the samples were visualized by illumination with polarized light to qualitatively further investigate collagen fibril orientation. The NP specimens removed and collected during the surgery after AF defect creation, and nucleus fenestration were stained with von Kossa staining to determine the amount of mineralization presented and interpreted as bone tissue deriving from surgical iatrogenic vertebral endplate trauma.

2.8 | Statistical analysis

Statistical analysis among the parameters of interest was performed with Prism version 8 for Windows (GraphPad Software, La Jolla, California). Descriptive data (mean ± SD, incidence or median and range) were provided. Differences in the percentage of disc height variation (in vivo CT), Pfirrmann grade (ex vivo MRI, grades obtained after consensus), and histological grading (for each parameter and total score) were assessed with nonparametric Friedman two-way analysis of variance for paired samples for IVD status (AF defect types: slit, cruciate, box-cut; intact control) with fixed effect of the sheep and respective observation periods. For all analyses, statistical significance was set at $p < 0.05$.

The reliability of the MRI Pfirrmann grading scheme was estimated using agreement percentage and kappa statistics within observers (intraobserver reliability) and between observers (interobserver reliability).[40] According to Landis and Koch,[41] the agreement was rated as follows: kappa 0–0.2 indicated slight agreement, 0.21–0.4 fair agreement, 0.41–0.60 moderate agreement, 0.61–0.8 substantial agreement, and 0.81 upward excellent agreement. With this rating, an absolute agreement would be 1. The 2 observers with less experience were removed from the interobserver reliability evaluation since they showed considerably poorer intraobserver reliability (Kappa of 0.072 and 0.385).

3 | RESULTS

3.1 | Animals and surgical intervention

The surgical intervention was successful in all sheep. Based on the histopathological analysis of the removed NP tissue, 60% of IVD ($n = 11/18$; similar distribution between the AF defect types) experienced some degree of iatrogenic endplate trauma judged minimal in

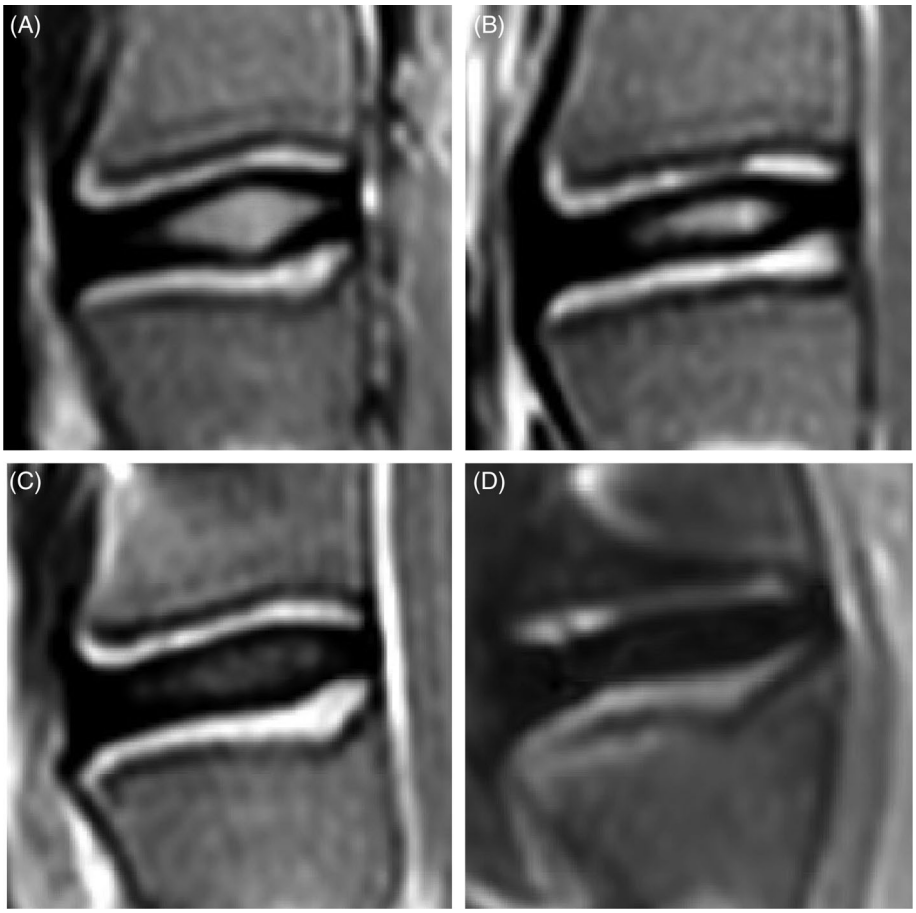

FIGURE 3 Pfirrmann grading system used to assess lumbar intervertebral disc (IVD) degeneration in a sheep annulus fibrosus (AF) defect and partial nucleus pulposus (NP) removal model. Grading using T2-weighted midsagittal MR images from a sheep model of injured lumbar intervertebral discs using 3 different annulus fibrosus status (control; slit, cruciate, box-cut AF defect) followed by a 0.1 g nucleus pulposus removal, performed according to the described grading used for human intervertebral discs from Pfirrmann et al.[38] (A) Grade I: The structure of the disc is homogeneous, with a bright hyperintense white signal intensity and a normal disc height. (B) Grade II: The structure of the disc is inhomogeneous, with a hyperintense white signal. The distinction between nucleus and annulus is clear, and the disc height is normal, with or without horizontal gray bands. (C) Grade III: The structure of the disc is inhomogeneous, with an intermediate gray signal intensity. The distinction between nucleus and annulus is unclear, and the disc height is normal or slightly decreased. (D) Grade IV: The structure of the disc is inhomogeneous, with an hypointense dark gray signal intensity. The distinction between nucleus and annulus is lost, and the disc height is normal or moderately decreased

all cases according to the histological analysis. Misalignment of the Steinmann Pin during its insertion into the lateral cortex of L2 led to contact with the spinal canal in one sheep from the 1-month observation group. This sheep was recovered from general anesthesia in a sling suspension system. The sheep was kept in the sling for 3 days postoperatively and hand an uneventful convalescence. No other complications were reported. No clinical signs of back pain were observed during the entire duration of the study based on clinical physical examination and welfare scoring results, and all sheep gained weight postoperatively.

3.2 | *In vivo* clinical CT

No to minimal degenerative changes with no to minimal new bone formation were observed at the lumbar spine for all sheep independently of the study group and AF defect (Figure 4A). The control IVD had a mean postoperative height variation of 102% ± 3%. The injured IVD had a mean postoperative disc height variation of 91% ± 5%, 89% ± 5%, and 89% ± 5% for the slit, cruciate, and box-cut AF defect, respectively. The postoperative disc height variation of injured IVD was significantly decreased (disc height loss) compared to control IVD immediately after the surgery and at 2 and 4 weeks postoperatively ($p = 0.0011$, 0.0086, 0.0056 postoperatively; $p = 0.0011$, 0.0007, <0.0001 at 2 weeks; $p = 0.0011$, 0.0011, <0.0001 at 4 weeks, for the slit, cruciate, and box-cut AF defect, respectively; Figure 4B). Twelve weeks postoperatively, the height variation of injured IVD was significantly decreased (disc height loss) compared to control IVD only for the cruciate and box-cut AF defect ($p = 0.00419$, 0.0295, for cruciate and box-cut AF defect, respectively). Furthermore, the only significant difference between the AF defect types was detected between the cruciate and box-cut defect ($p = 0.0304$) at 12 weeks

TABLE 2 Histopathological evaluation

Grade	Definition
Proteoglycan depletion based on Safranin O-Fast Green-staining	
0	Fast green staining only of outer AF, intermediate Safranin O staining of inner AF, intense Safranin O staining in NP, well defined cartilaginous endplate staining. Alternate AF lamellae discernable due to differing Fast Green staining intensities of adjacent lamellae
1	Fast green staining only of outer AF, intermediate Safranin O staining of inner AF, intense Safranin O staining in NP, well defined cartilaginous endplate staining. Alternate AF lamellae discernable due to differing Fast Green staining intensities of adjacent lamellae
2	Moderately reduced Safranin O staining of mid and inner AF in vicinity of lesion, fast green staining of outer AF only, normal Safranin O staining of NP and cartilaginous endplate
3	Reduced patchy Safranin O staining around lesion, fast green staining in outer AF
4	Reduced Safranin O staining in NP compared to control IVD, very faint or no Safranin O staining in mid and outer AF, fast green staining only in outer AF
IVD structure and lesion morphology	
0	Normal IVD structure with well-defined annular lamellae, central NP and cartilaginous endplate
1	Lesion evident in mid AF, normal NP morphology
2	Lesion evident in mid and inner AF, but may not be apparent in outer AF due to spontaneous repair, inner AF lamellae may be inverted and have anomalous distortions in normal lamellar architecture
3	Bifurcation/propagation of lesion from mid to inner AF into NP margins, mild delamination, when more extensive may lead to concentric tears between lamellae in mid and inner AF
4	Propagation of lesion into NP, with disruption in normal NP structure, distortion of annular lamellae into atypical arrangements-severe delamination, separation of translamellar cross bridges
Cellular morphology	
0	Normal, sparse distribution of typical single AF and NP fibrochondrocytes
1	Small groups of rounded chondrocytic cells (2–4 cells/group) in vicinity of annular lesion in inner AF, occasional cell division in resident inner AF and NP cells
2	Moderate increase in well-defined groups of rounded chondrocytic cells (4–8 cells/group) in vicinity of lesion and with penetrating blood vessels associated with the lesion site, well defined chondroid cell colonies in NP contained within a dense basophilic matrix with little fibrillar material evident around the cells contrasting with NP cells
3	Marked increase in less defined groups of rounded chondrocytic cells (>8 cells/group) in vicinity of lesion and with penetrating blood vessels associated with the lesion site, well defined chondroid cell colonies in NP (<50 cells/colony) contained within a dense basophilic matrix with little fibrillar material evident around the cells contrasting with NP cells
4	Numerous cell clones around inner and mid AF lesion, chondroid cell nests in NP containing >50 cells
Blood vessel ingrowth	
0	Very occasional vessels in outermost annular lamellae, occasional capillaries in cartilaginous endplate
1	Slight influx of cells mainly in outer AF
2	Moderate influx of cells throughout AF
3	Large influx of cells throughout AF
4	Extensive influx of cells throughout AF particularly in inner AF and around lesion
Cellular influx into lesion	
0	Normal cell distribution in mid, inner and outer AF, and NP
1	Slight influx of cells mainly in outer AF
2	Moderate influx of cells throughout AF
3	Large influx of cells throughout AF
4	Extensive influx of cells throughout AF particularly in inner AF and around lesion
Cleft formation in vicinity to lesion	
0	No clefts in AF
1	Small cleft area in AF
2	Moderate cleft area in AF
3	Large cleft area in AF
4	Vast cleft area in AF and also in NP

Note: Histopathological features for histopathological semiquantitative grading for the evaluation of IVD degeneration performed on sections of control and injured IVD. Adapted from Shu et al.[39]

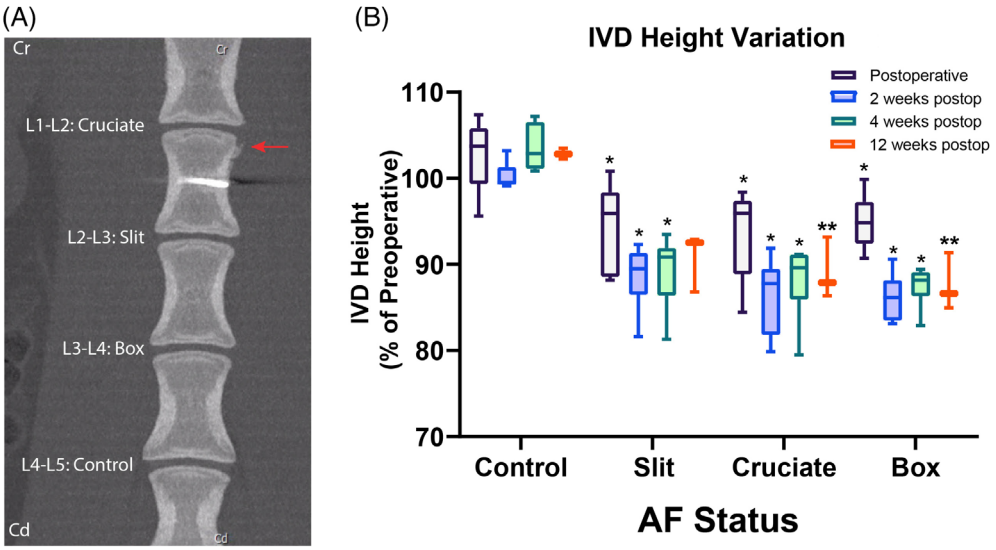

FIGURE 4 Computed tomography (CT) imaging shows IVD height loss in all 3 defect types. (A) CT image and results from a sheep model of injured lumbar intervertebral discs using 3 different annulus fibrosus (AF) status (control; slit, cruciate, box-cut AF defect) followed by a 0.1 g nucleus pulposus (NP) removal. Representative coronal CT image of a sheep lumbar spine 3 months after AF defect and partial NP removal showing no to minimal degenerative changes of injured disc with mild periosteal proliferation (arrow). (B) Histogram demonstrating the variation in postoperative total disc height expressed in percentage of height variation (%) compared to respective preoperative disc height according to the AF status (intact control; slit, cruciate, box-cut AF defect injury) at each observation period (postoperative, 2 weeks, 4 weeks, and 12 weeks postoperatively). Within the same observation period, asterisks indicate a significant difference in height variation of the injured AF (slit, cruciate, box-cut AF defect) compared to control ($p < 0.05$). Additionally, double asterisks indicate a significant difference between the AF status at 12 weeks postoperatively. The analysis is based on 6 IVD per AF status (pooling the 3 different IVD levels) for all observation periods except the 12 weeks postoperatively, which was based on 3 IVD per AF status

postoperatively, with the box-cut defect showing a more pronounced disc height loss (Figure 4B).

3.3 | *Ex vivo* MRI

The comprehensive evaluation of lumbar IVD revealed no abnormalities of the control IVD among the evaluated parameters. The injured IVD showed qualitatively decreased disc height with no signs of herniation, protrusion, or extrusion (Figure 5A). Disc bulging, seen as disc tissue extending beyond the edges of the ring apophyses throughout the circumference of the disc, qualified as asymmetric was detected in 83% of injured IVD and appeared equally distributed among the AF defects ($n = 5/6$ per AF defect). Diffuse bulging was detected in 1 injured IVD that belonged to the box-cut AF defect. Loss of AF morphology or annular fissure (Figure 6) was visible in 83% of IVD injured with the cruciate and box-cut AF defects ($n = 5/6$ per AF defect) and 67% of IVD injured with slit AF defect ($n = 4/6$). Changes in signal intensity involving at least one of the vertebral endplates of the evaluated IVD, associated with signs of degenerative or inflammatory changes, were detected in all injured IVD but 1 from the slit AF defect.

Even in the absence of injury creation, mild disc degeneration according to Pfirrmann grading was noted for all control IVD (median grade 1; Figure 5B). More pronounced degenerative changes were observed in the injured IVD indicated by the significantly higher Pfirrmann grade of the injured IVD (median grade of 3 for all AF defects, range 1–4) compared to control IVD ($p = 0.0022$, 0.004, 0.0256 for the slit, cruciate, box-cut AF defect respectively; Figure 5B). No difference was detected between the different types of AF defects ($p = 0.2327$, 0.7567, 0.4630).

The intraobserver agreement percentage of the Pfirrmann grading varied from 42% to 83% among the observers. The experienced board-certified veterinary radiologist showed the greatest intraobserver reliability with the highest agreement percentage (83%) and substantial kappa agreement (kappa 0.745, 95%IC 0.530–0.961). The most experienced surgeon showed the second greatest intraobserver reliability with a 71% agreement percentage and moderate kappa agreement (kappa 0.473, 95%CI 0.204–0.743). The 2 least experienced surgeons (removed from the interobserver analysis) showed the lowest intraobserver reliability with low agreement percentages (42 and 62%) and slight to fair kappa agreement (kappa 0.072, 95%IC -0.235-0.379, and 0.385, 95%IC 0–065-0.705). The interobserver agreement (2 observers) was 75% with a moderate kappa agreement (kappa 0.546, 95%CI 0.279–0.812).

3.4 | Histological analysis

All injured IVD showed a combination of defects involving the AF and NP without signs of herniation, along with degenerative and inflammatory alterations and limited reparative changes (Figure 7A). Common changes characterizing the injured IVD were depletion of proteoglycan content, severe morphological changes in AF and NP, blood vessel ingrowth, influx of inflammatory cells, and cleft formation

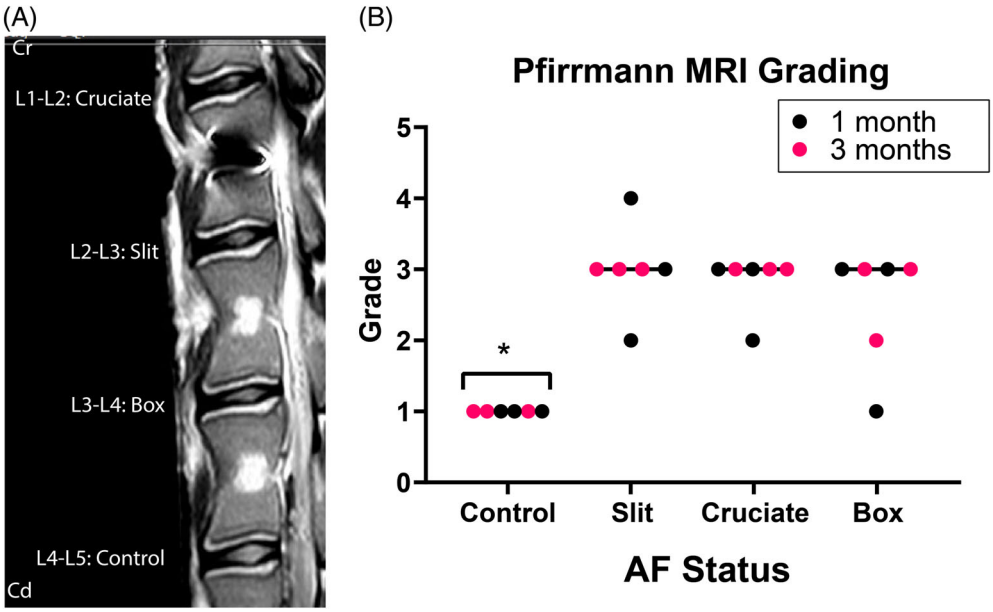

FIGURE 5 Magnetic resonance (MR) imaging shows increased degeneration grade for all defect types. MR image and results from a sheep model of injured lumbar intervertebral discs using 3 different AF status (control; slit, cruciate, box-cut AF defect) followed by a 0.1 g NP removal. (A) Representative T2-weighted midsagittal MR image from the same sheep lumbar spine as from Figure 4 taken 3 months after annulus fibrosus (AF) defect and partial nucleus pulposus (NP) removal. (B) Scatter plot demonstrating the Pfirrmann grading according to the AF status (intact control; slit, cruciate, box-cut AF defect injury) after 1-month (red) and 3-month (black) observation period. The line of each AF status represents the grand median. Asterisks indicate a significant difference between the AF status ($p < 0.05$). The analysis is based on 6 IVD per AF status (pooling the 3 different IVD levels and both observation periods)

(Figure 8). The structural changes of the AF and the NP of injured IVD were recorded at high severity (median 3 for slit and box-cut AF defect and 3.5 for cruciate AF defect) and were characterized by distortions of the AF lamellar structure (Figure 8A,B), concentric tears between lamellae propagating into NP margins, and delamination and separation of trans-lamellar cross-bridges in 4 IVD. Blood vessel ingrowth was observed within the AF and into the NP to a lower extent (Figure 8E). Changes in cell morphology were observed in both intact control and injured IVD and were characterized by the formation of nests of rounded chondrocytic cells with denser matrix and decreased amount of fibrillar material surrounding them (Figure 8F). The injured IVD had a statistically significant increase in total histological score compared to control IVD (Figure 7B; $p = 0.0004$, 0.006, 0.0009 for the slit, cruciate, and box-cut AF defect, respectively). However, no significant difference was detected between the types of AF defect created ($p = 0.1456$, 0.2970, 0.9725).

4 | DISCUSSION

The present study characterized a preclinical sheep IVD injury model capable of mimicking degenerative human spinal pathology. The evaluation of 3 frequently used sheep IVD injury models showed that all surgical techniques combining AF defect creation (slit, cruciate, or box-cut AF defect) followed by partial NP removal reproducibly produced short-term disc height loss (up to 1 month postoperatively), MRI signs of disc degeneration (Pfirrmann grading), and semiquantitative histopathological assessment of disc degeneration degree. However, the long-term disc height loss differed between the AF defect types at 3 months postoperatively, where disc height was restored to preoperative values in the slit AF defect, and disc height loss became more pronounced in the box-cut compared to the cruciate AF defect. All surgical techniques were able to produce bulging of disc tissue beyond the edges of the ring apophyses; however, none was capable of producing disc herniation.

4.1 | Overview and study period

The complexity of human disc degeneration does not allow any animal model to perfectly mimic the clinical pathophysiological process. Even though spontaneous disc degeneration has been described in animal models using rodents and chondrodystrophic dogs,[42] IVD injury is usually initiated by compromising IVD structural integrity using various chemical solutions such as chondroitinase,[43] inducing abnormal mechanical loading to the spine[44] or surgically creating mechanical injury.[14] The IVD injury models evaluated in this study are defined as structural models in which direct physical methods were used to induce disc degeneration by precisely compromising the AF and NP structural integrities of the IVD. Such large animal models of disc degeneration are considered to reproduce many important characteristics of the pathobiology of disc degeneration in humans.[14,16] The chosen methodology involving full-thickness AF injury is known to produce nuclear avulsion with relatively rapid IVD degeneration.[45] In

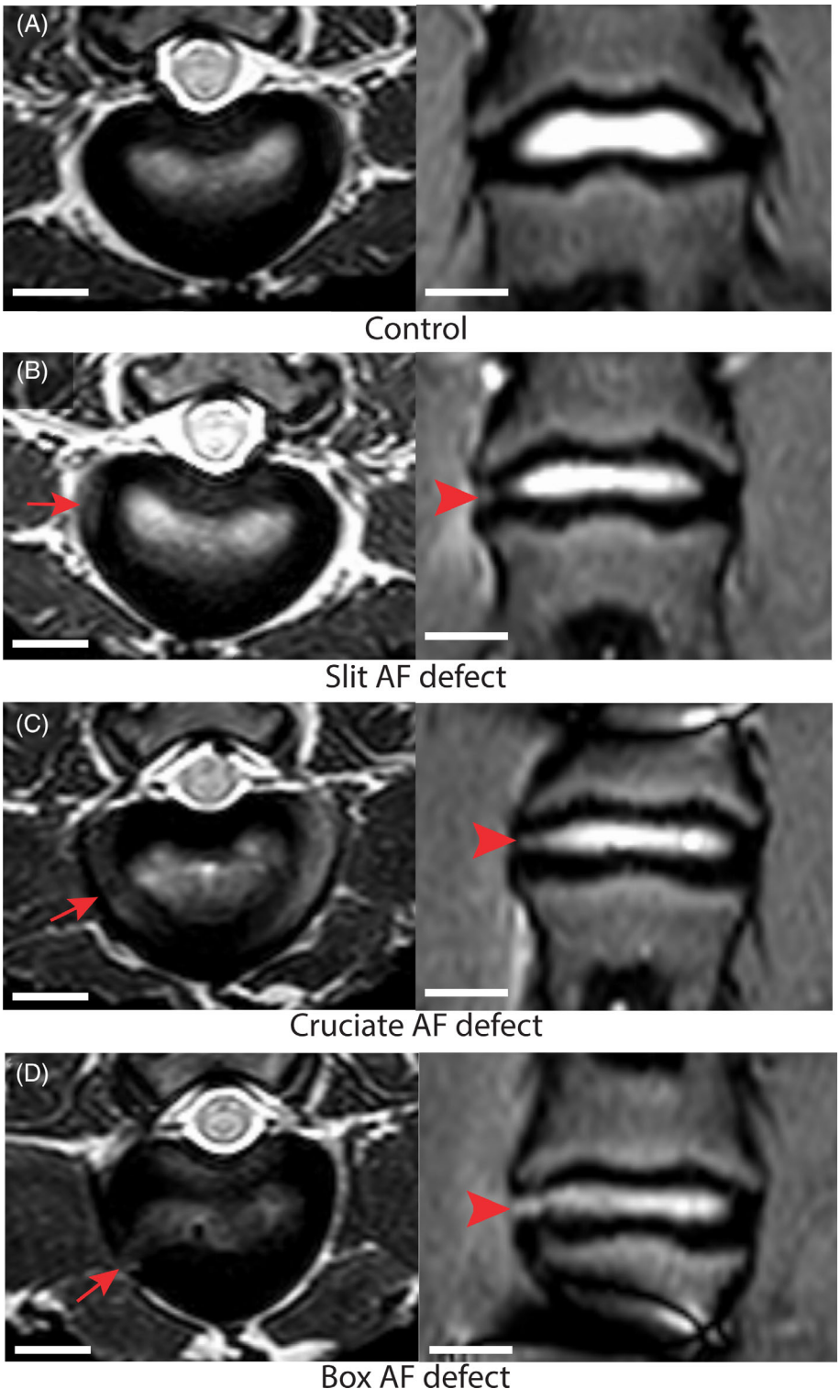

FIGURE 6 Magnetic resonance (MR) imaging identified AF fissures in all defect types. Representative MR T2-weighted transverse (left) and Short-Tau Inversion Recovery turbo spin echo coronal (right) MR images changes observed from a sheep model of injured lumbar intervertebral discs (IVD) using 3 different annulus fibrosus (AF) status (control; slit, cruciate, box-cut AF defect) followed by a 0.1 g nucleus pulposus (NP) removal taken 3 months after surgery. The images are illustrating annular fissure characterized by loss of the morphology of the AF characterized by separation between the annular fibers (arrow and arrowhead) in the injured IVD; scale bar: 1 cm

contrast, a partial-thickness injury would likely have produced a slower degenerative process over several months from the initiation of progressive failure of the inner annulus to progressive IVD degeneration.[14] The ability of IVD injury models to produce a short and predictable time course of disc degeneration has several advantages. Predictable and fast models increase the models' reliability in the investigation of potential therapies, allow targeting a specified time point of treatment, and reduce the cost concerns of regenerative therapy studies. An important consideration in any prospective treatment study is whether it will be useful and effective during early acute and later acute stages of IVD degeneration or in more established chronic stages of the disease.

To address the usefulness of each injury model, two observation periods were studied to simulate the early (1 month) and late acute

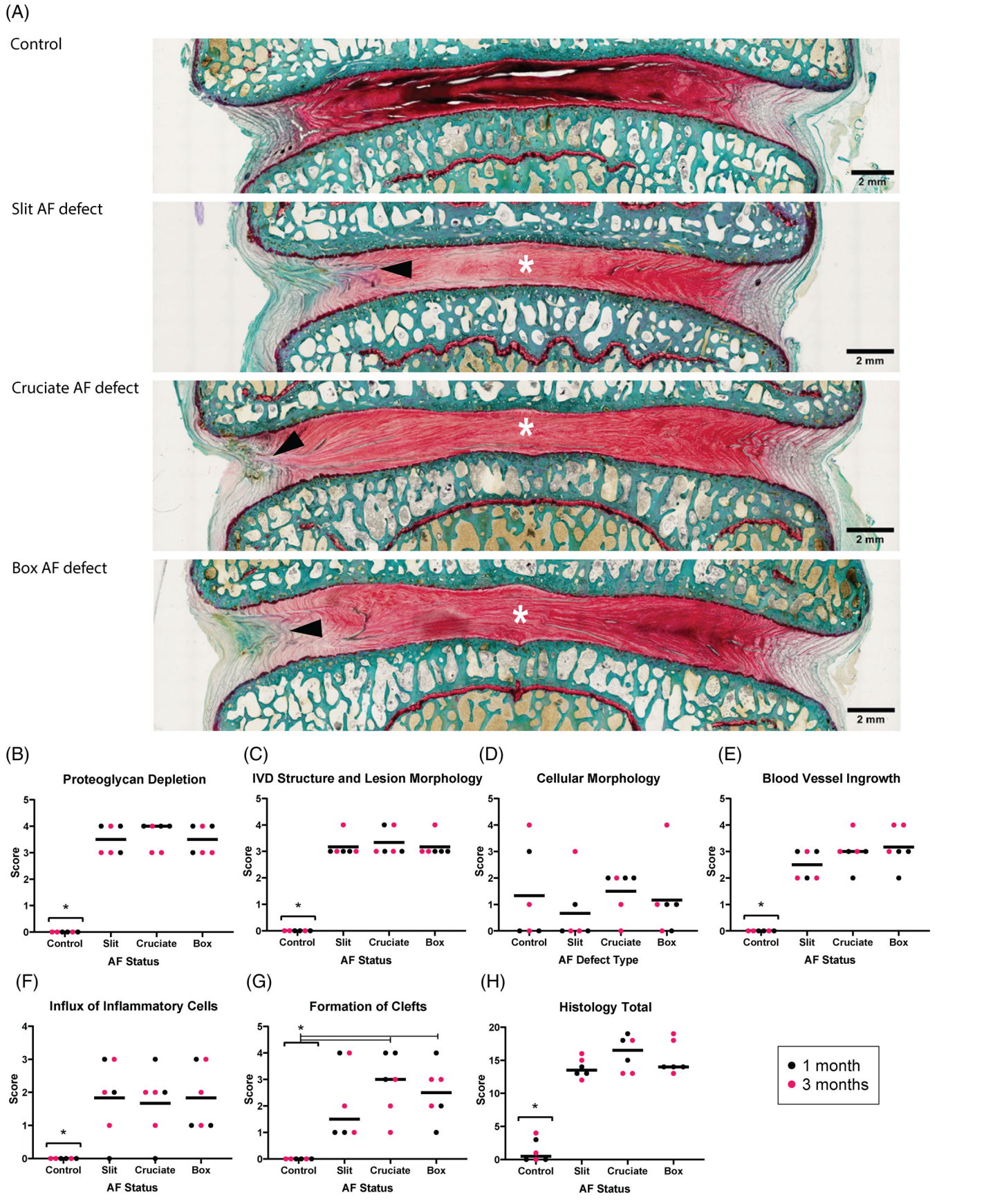

FIGURE 7 Legend on next page.

(3 months) stages of the IVD degeneration process. The sheep from the 3 months observation period showed no clinical difference and similar increases in Pfirrmann grading and histopathological score in relation to the sheep from the 1 month observation period, possibly reflecting the acute onset of IVD degeneration postoperatively without significant evolution of the condition after the first month. There were no added benefits in a longer induction period of 3 months with the cruciate and box-cut defects and a loss of significance in postoperative disc height variation with the slit AF defect compared to the preoperative control. Thus, early observation periods, particularly when using slit AF defect, may be more beneficial.

4.2 | IVD injury model: AF defect and NP removal

The AF defects used in this study are commonly used during routine discectomy procedures in humans. Box-cut AF excision is the most common annular entry used during postlumbar discectomy, followed by slit type and cruciate incisions.[46] The severity (width and depth) of the AF defects evaluated in this study was based on previously published models capable of inducing some level of degenerative changes in sheep.

The first sheep AF lesion model was developed by Osti et al.[14] and employed a 5 mm width and 5 mm depth slit AF defect.[34–36] This model provided valuable understandings of temporal extracellular matrix changes that occur following induction of AF lesions, yet is limited by the slow development of pathological changes, which occur across a 12- to 18- month period. The severity of this slit model was later increased by adding NP removal or modifying the defect dimensions. The addition of NP removal to the slit model can accelerate the development of pathological changes as early as 6 weeks postoperatively, as showed by Reitmaier et al.[22] More severe slit AF defect done by a longer incision (20 mm width) was also shown to accelerate the development of pathological changes detectable 12 weeks postoperatively.[16–18,47] In order to standardize the NP removal procedure across the surgical techniques tested to create injured IVD, a slit AF defect with moderate severity (width 16 mm) combined with NP removal was chosen for our study.

In the past decades, new sheep IVD injury models were developed using box-cut AF defects. Even though all models portrayed degenerative changes, the severity of the described box-cut AF defects fluctuates greatly.[12,13,19–21] The described severities vary from the removal of a 3.5 mm × 3.5 mm AF box-cut without NP removal[21] to a 3.0 mm × 10 mm AF box-cut with NP removal.[13] Because of the large variation between the models, an AF box-cut defect frequently used in IVD injury models with moderate severity (5 mm × 3 mm)[19–21] was chosen. Similarly to the slit AF defect, this injury was combined with NP removal, also frequently performed concurrently with the box-cut AF defect.[20,21,48] On the contrary to the slit and box-cut AF defect, the cruciate AF defect has been less investigated in sheep IVD injury models.[48] Despite its lesser popularity in sheep, the cruciate AF defect was included in this study because of its common usage as annular entry during postlumbar discectomy.[46]

NP removal in sheep IVD injury models is not always necessary to produce degenerative changes within the operated IVD.[11–18] Following AF injury, the damaged outermost AF will undergo active remodeling, while the inner AF remains unhealed leading to matrix metalloproteinases driven degenerative changes ultimately resulting in IVD degeneration.[49] While this series of events closely resemble events that occur in humans' IVD degeneration, NP removal was performed in this study in conjunction with all AF defects to better mimic human spinal pathologies with routine discectomy.[46] When performed, the reported quantity of NP removed in sheep IVD injury models generally vary between 0.1 g[13,19] and 0.2 g.[20–22] In this study, the weight of NP removed was standardized to 0.1 g to increase the chance of postoperative herniation. In fact, radical removal of disc material is known to decrease the possibility of reherniation after a discectomy procedure by minimizing the chance that the remaining NP material might become the source of another disc protrusion.[9,50] However, preserving too much NP material could decrease the likelihood of detecting disc height changes.[50,51]

4.3 | Disc material herniation

None of the defects created in this study successfully produced disc herniation, defined as a focal displacement of disc material (≤25% of the disc circumference) beyond the limits of the IVD space. In most injured IVD, NP material was visible within the AF defect (Figure 6B), which meant that it was displaced beyond its normal anatomical location. However, according to the herniation definitions used in this study (Table 1) and based on the human MRI reherniation classification scheme,[52] this finding would not be classified as herniation since the disc material did not break through the confines of the AF (only found within) or was found beyond the normal outer limits of the disc. The lack of disc material herniation is in concordance with most sheep

FIGURE 7 Histopathological grading shows increased IVD degeneration grades in all defect types. Histology results from a sheep model of injured lumbar intervertebral discs (IVD) using 3 different annulus fibrosus (AF) status (control; slit, cruciate, box-cut AF defect) followed by a 0.1 g nucleus pulposus removal. (A) Control sample showing highly aligned AF lamellae compared to injured samples (intact control; slit, cruciate, box-cut AF defect injury) showing reduction of staining (region of white asterisk) and discontinuous AF tissue (black arrowhead) (nondecalcified, resin-embedded, Safranin O-Fast Green-stained material; scale bar: 2 mm; images taken in dorsal plane. Orientation: left is left ventrolateral and bottom is caudal). (B–H) Scatter plots demonstrating the semiquantified histological findings according to the AF status (intact control; slit, cruciate, box-cut AF defect injury) after 1-month (red) and 3-month (black) observation period. The line of each AF status represents the grand median. Asterisks indicate a significant difference between the AF status ($p < 0.05$). The analysis is based on 6 IVD per AF status (pooling the 3 different IVD levels and both observation periods)

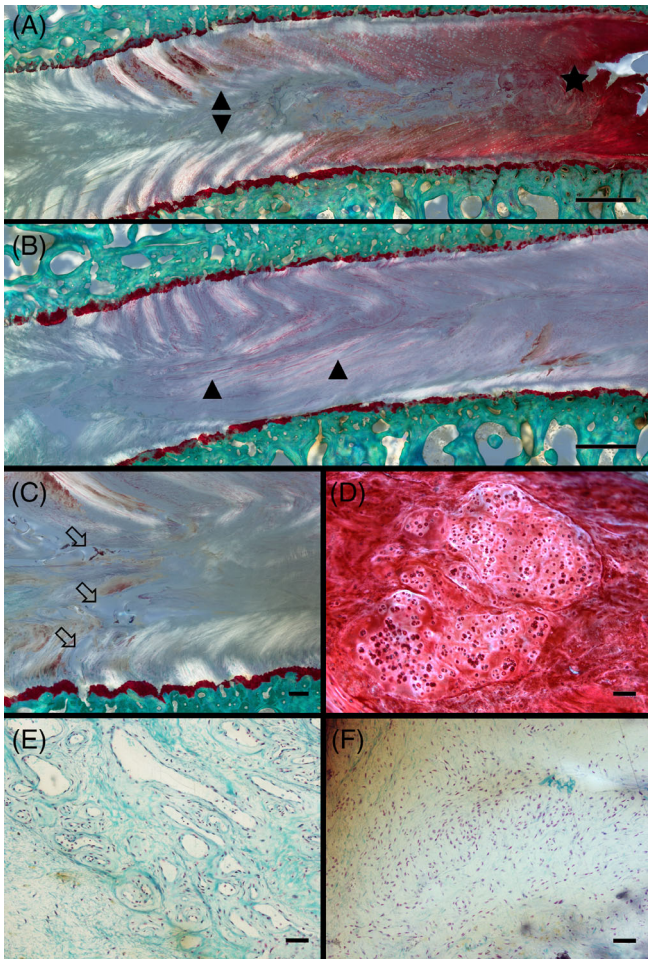

FIGURE 8 Microscopical evaluation showed intervertebral discs (IVD) degeneration changes in all defect types. Representative microscopical changes observed during histopathological grading from a sheep model of injured lumbar IVD using 3 different annulus fibrosus (AF) status (slit, cruciate, box-cut AF defect) followed by a 0.1 g nucleus pulposus (NP) removal. (A-B) Severe morphological changes in the AF and NP visualized by illumination with polarized light characterized by a disruption and de organization of the structured annular lamellae (delamination; arrowheads). Depletion of proteoglycan content of the AF and part of the NP regions demonstrated by markedly reduced Safranin O staining (asterisk) compared to a normal intensely stained region is also observed; scale bar: 1 mm. (C) Cleft formation visualized by illumination with polarized light characterized by complete discontinuation of fibrils leading to the formation of voids (open arrows); scale bar: 200 μm. (D) Changes in cell morphology characterized by the formation of differently sized clusters of rounded chondrocytic cells; scale bar: 100 μm. (E) Blood vessel ingrowth characterized by small capillaries in close vicinity of an IVD defect (not shown in the picture); scale bar: 50 μm. (F) Influx of inflammatory cells characterized by aggregation of round to oval lymphocytic cells in close vicinity of an IVD defect (not shown in the picture); scale bar: 50 μm. (nondecalcified, resin-embedded, Safranin O-Fast Green-stained thick-sections)

IVD injury models that did not report nucleus herniation after AF defect creation.[11,15–22,47]

In human discectomy patients, unrepaired larger annulus defect sizes are associated with a higher rate of disc reherniation.[50,53] Furthermore, large AF tissue defects are associated with the highest reoperation with a rate of up to 21% because of reherniation.[9] It was hypothesized that sheep IVD following discectomy would act in a similar fashion as human IVD since the sheep is of a roughly similar size to humans and, despite its quadrupedal posture, is exposed to very similar mechanical stresses to the human IVD.[54] The fibrosity of the NP could play a role in the different rates of disc herniation between species. While there are no studies directly comparing the fluidity or fibrosity of human and sheep NP to the best of the authors' knowledge, needle puncture has been reported to induce NP leakage in pigs,[55,56] rats,[24,57] and rabbits[58] while mechanical tools are required to remove NP in sheep.[13,19–22] This could suggest that the fibrous NP of sheep may be less prone to herniation compared to more fluid NP. Another possible explanation of the different rate of disc herniation following discectomy procedure between humans and sheep is the discrepancy in the preoperative status between human patients, frequently presented with disc herniation prior to the surgical procedure, and laboratory sheep found to be free of degenerative diseases prior to inclusion in the study. Study cohorts of human patients probably possessed more risk factors such as age[50] and body mass index[59] known to increase the risk of postoperative disc herniation compared to healthy laboratory sheep. The relatively short observation period (up to 3 months) could also have reduced the chances to detect disc herniation considering the mean time to the first reoperation of 7.8 ± 6.7 months after primary discectomy in human patients.[46]

The surgical technique used is another possible explanation of the different rate of disc herniation following discectomy procedure between humans and sheep[60] It was previously observed that human discectomy patients whose defects were wider than 6 mm had a 27% rate of documented reherniation compared to 5% in the remaining patients of the same cohort.[9] Similarly, discectomy patients with AF defect greater than 54 mm^2 had a 15% rate of reherniation compared to 5% for patients with defect sizes less than 36 mm^2.[50] Despite the fact that the slit and cruciate AF defects created in this study were wider than 6 mm, none of the defects produced an AF defect greater than 36 mm^2. A sheep IVD injury model that created a box-cut defect with twice of the area of AF removed compared to the defect created in this study (10 mm × 3 mm; 30 mm^2 vs. 5 mm × 3 mm; 15 mm^2) was capable of producing disc herniation and in some cases disc sequestration.[13] Despite better mimicking human discectomy procedures, the removal of NP material (0.1 g) could have decreased the likelihood of disc herniation. Radical human discectomy procedures have been shown to reduce the risk of postoperative herniation compared to limited discectomy by decreasing the amount of disc material left in situ capable of reherniate.[9,50] However, sheep IVD injury models with similar AF defects and without NP removal also failed to produce detectable disc herniation postoperatively.[11,16,18,47]

4.4 | Disc height loss and CT changes

In human patients, degenerating IVD are observed to lose disc height over time because of NP dehydration and tissue loss, resulting in a

reduced capacity to resist the compressive loads applied to the spine.[18] The postoperative loss of total disc height was a consistent finding across all AF defect types in the shorter term (up to 1 month postoperatively). The 10% average loss of disc height is slightly lower compared to other sheep IVD injury models that reported an average loss from 20% to 30%.[11,17,20,21,47] The methodology used in this study to measure disc height loss, which was different from the methodology used in other sheep studies, was chosen to minimize the influence of minor variation in vertebral position from sheep positioning during CT scan examination but could have caused the differences in relative measurements in this study. The difference in disc height loss across the studies could also reflect the impact of different amounts of NP removed.[50,51] The recovery of disc height similar to uninjured control IVD 3 months postoperatively in the slit AF defect is an interesting result. This finding showed that not all AF defects are equal and are an important consideration in research protocol creation for any prospective treatment intended to be effective during early acute, later acute, or established chronic stages of degeneration.

The difference observed with the slit AF defect could result from a less invasive disruption of the AF compared to the cruciate and box-cut AF defects. It has been previously shown that a slit AF incision, judged as a less-invasive AF disruption, retained a better ability to withstand internal pressurization and to resist changes in corresponding multidirectional vertebral motion than a full-thickness box-cut AF excision.[61] The stronger AF healing after transverse slit AF incision compared to more invasive AF defects was hypothesized to be a consequence of better preservation of local blood supply found in the outer annulus and of more intact AF fibers.[61] These factors would also result in faster AF repair in slit AF defects compared to cruciate and box-cut defects, which could be reflected by restoration of disc height similar to uninjured control IVD at earlier time points. Pressure–volume studies used to assess the healing strength of IVD, comparing slit, cruciate, and box-cut AF defects in a sheep IVD injury model support this hypothesis. The slit-incised discs showed a significant increase in strength from 2 weeks (740 kPa) to 6 weeks (1410 kPa) and were shown to withstand up to twice the amount of internal pressurization without fluid leakage through the AF defect compared to box-incised disc.[48] Transverse slit AF incision reproducibly introduces small defects, which could mimic early AF lesions and be more supportive of tissue healing compared to more severe AF defects.

4.5 | MRI Pfirrmann grading

MRI is a common clinical imaging modality used to investigate cases of back pain and evaluate IVD status in human patients. The T2-weighted sequence allows investigation of the anatomical structures and IVD hydration.[55] In this study, T2-weighted and T2-weighted short-tau inversion recovery (STIR) MR images allowed visualization of similar AF and NP morphology changes and annular fissure between the different AF defect types. Quantitative image analysis using Pfirrmann grading, a ranked-based approach to evaluate the severity of IVD degeneration using axial and sagittal T2-weighted MR-images,[38] further supported the qualitative MRI findings. The ability of the different AF defects to precipitate IVD degeneration is a critical aspect to be considered for preclinical IVD degeneration studies. For this reason, Pfirrmann grading is frequently used as a primary outcome in sheep IVD injury studies.[17–19,21,33,47] All AF defects combined with NP removal reliably induced T2 signal changes and generated MR-images compatible with IVD degeneration resulting in an increased Pfirrmann grading. However, the similarity of the results between 1 and 3 months postoperatively is limiting our ability to clearly differentiate between induction and progression of IVD degeneration mimicking human pathology and initiation of MRI signal changes due to structural damage inflicted. The Pfirrmann grading score of 1 noted in all control IVD in all sheep suggests mild signs of IVD degeneration despite the lack of IVD injury. Although it is impossible to draw a conclusion from the analyzes carried out in this study, the mild degeneration observed in the control IVD was believed to be most likely to be part of the natural aging process in the sheep than resulting from IVD injury in the adjacent level effects.

In this study, only the experienced board-certified veterinary radiologist had an intraobserver agreement using the Pfirrmann grading system (83%), similar to what is reported in human reliability studies (average of 85%).[56] The substantial intraobserver agreement difference between one of the human surgeons and veterinary radiologist (42 vs. 85%) could reflect the increased difficulty for the trained human surgeons to differentiate between degenerative changes and normal sheep IVD geometry and morphology. In fact, the geometry of sheep IVD was analyzed for similarities with human IVD with regard to 3 normalized parameters (disc height scaled by lateral width, the AF width scaled by lateral width, and the NP area scaled by disc area) and showed an overall 31% discrepancy between sheep and human IVD.[62]

The low interobserver agrees for the Pfirrmann grading in this study can be considered a potential limitation of this outcome measurement and highlights the importance of involving veterinary specialists in preclinical studies. The evaluation of MR images more than once by all observers and by at least 2 observers to assess Pfirrmann grading should be highly considered for all sheep IVD injury models and intra- and interobserver agreement reported and enhanced training on Pfirrmann grading for animal model analysis is an important consideration.

4.6 | Histopathological changes

Histological results demonstrated relative equivalency between 1- and 3-month observation periods. In this study, a scoring scheme sensitive to injured IVD and created for sheep control and treated AF defect was used.[39] Since the structural damage inflicted to the IVD structures in this study was more severe, the total histological score could be underestimated compared to simple AF defect models. There were no semiquantitative differences between the different AF defect types except for the cleft formation score, which was higher in

cruciate and box-cut AF defect compared to the slit, suggesting similar degenerative and natural repair processes. The lack of significant difference in cleft formation scores between control and injured IVD with the slit AF defect is also supporting the repair hypothesis explaining the earlier restoration of normal disc height observed on CT scan 3-month postoperatively with the slit AF defect. Interestingly, the cellular morphology score characterized by the formation of differently sized groups/nests of rounded chondrocytic cells was the only parameter similar for all AF statuses, including intact control IVD. It was therefore believed that this parameter was not a pathological change but an incidental background finding in adult sheep lumbar IVD. The increase in blood vessel ingrowth and the influx of inflammatory cells observed likely is a consequence of the AF injury with limited repair reaction and a sign for the ongoing degenerative process.[63,64]

The lack of significant differences in total histological score between the AF defects showed that they act similarly in terms of histological degeneration and repair process over a 1- to 3-month observation period. However, it is important to note that individual parameters such as cleft formation may be different between AF defects.

4.7 | Welfare assessment and pain

An important aspect of any preclinical animal study is the assessment and control of generated pain. European Union directive for the protection of animals used for scientific purposes requires an exact severity assessment of all procedures undertaken on laboratory animals. A study-specific scoring sheet based on clinical investigation performed by experienced veterinary personnel was used in the present study and included the evaluation of the feeding habits, animal behavior, posture, and ambulation. The individual score sheets did not demonstrate any clinical sign of postoperative pain in any of the sheep. In humans, lower back pain is a very common phenomenon and can result from nociceptive stimulation of the richly innervated paradiscal tissues, facet joints, and vertebral bodies.[65] Because of the similar nerve ingrowth during disc degenerative process and comparable IVD innervation between sheep and humans,[66–68] it would appear reasonable to expect that the painful stimuli from the procedure would be similar in sheep and in humans. The current inability to discern pain or changes in gait and ambulation in sheep in which IVD degeneration has been induced must be considered a limitation of this model and preclinical IVD research in general. The development of more tailored/specific methods and parameters to assess pain in IVD degeneration models would improve their scientific value.

4.8 | Limitations

The relatively low sample size is a potential limitation of this study. Nevertheless, this was sufficient to identify a significant effect on variables measured and reduced the need to sacrifice more animals, but a larger sample size may be needed to assess additional variables and provide broader generalizability across the studies.

The use of Swiss White Alpine sheep may limit direct comparisons with some of the earlier preclinical studies using different sheep breeds such as Merino sheep. While the macroscopical evaluation of the IVD included gross morphological and imaging outcomes, the mechanical functional effect of the different AF statuses was not evaluated. The lack of biomechanical evaluation may have limited the ability to detect differences between the AF status and decreased the translational applicability to human injured IVD. Similarly, the microscopical evaluation of the IVD was limited to histological analysis of tissue sections to assess the microstructure and degenerative changes. The inclusion of immunohistochemical evaluation would have provided a more objective assessment compared to the histological grading schemes used that may depend on the individual observer.

5 | CONCLUSION

This study clearly showed that all AF defects, when combined with NP removal, led to significant degenerative changes detectable using medical imaging techniques and histopathological analysis as early as 1 month postoperatively and for up to 3 months postoperatively. The tested AF defects (slit, cruciate, and box-cut AF defects) were not equal in terms of disc height loss at 3 months postoperatively, with the slit AF defect showing restoration of normal disc height and box-cut defect creating the greatest disc height loss, which is an important factor to take into consideration in research protocol creation for any prospective treatment. While all surgical techniques were able to produce bulging of disc tissue beyond the edges of the ring apophyses, none was capable of producing disc herniation, a pathology commonly reported in humans after a discectomy procedure.

ACKNOWLEDGMENTS

The author would like to show gratitude to Nora Goudsouzian, Dr Thomas P. Schaer and Dr Bertrand Lussier who provided insight and expertise that greatly assisted the research, and J&J Medical Devices for their technical assistance by providing the DePuy Synthes SynFrame Retractor System.

CONFLICT OF INTEREST

The authors declare no conflict of interest

ORCID

Caroline Constant https://orcid.org/0000-0002-7846-5612
Dirk Nehrbass https://orcid.org/0000-0002-4871-5473
Sibylle Grad https://orcid.org/0000-0001-9552-3653
James C. Iatridis https://orcid.org/0000-0002-2186-0590

REFERENCES

1. Anema JR, Schellart AJ, Cassidy JD, Loisel P, Veerman TJ, van der Beek AJ. Can cross country differences in return-to-work after

chronic occupational back pain be explained? An exploratory analysis on disability policies in a six country cohort study. *J Occup Rehabil*. 2009;*19*(4):419-426.
2. Becker A, Held H, Redaelli M, et al. Low back pain in primary care: costs of care and prediction of future health care utilization. *Spine (Phila Pa 1976)*. 2010;*35*(18):1714-1720.
3. Ito K, Creemers L. Mechanisms of intervertebral disk degeneration/injury and pain: a review. *Global Spine J*. 2013;*3*(3): 145-152.
4. Whatley BR, Wen X. Intervertebral disc (IVD): structure, degeneration, repair and regeneration. *Mater Sci Eng C*. 2012;*32*(2):61-77.
5. Boden SD, Davis DO, Dina TS, Patronas NJ, Wiesel SW. Abnormal magnetic-resonance scans of the lumbar spine in asymptomatic subjects. A prospective investigation. *J Bone Joint Surg Am*. 1990;*72*(3): 403-408.
6. Singh K, Masuda K, Thonar EJMA, An HS, Cs-Szabo G. Age-related changes in the extracellular matrix of nucleus pulposus and anulus fibrosus of human intervertebral disc. *Spine*. 2009;*34*(1):10-16.
7. Weinstein JN, Lurie JD, Tosteson TD, et al. Surgical versus nonoperative treatment for lumbar disc herniation: four-year results for the spine patient outcomes research trial (SPORT). *Spine (Phila Pa 1976)*. 2008;*33*(25):2789-2800.
8. Rihn JA, Hilibrand AS, Radcliff K, et al. Duration of symptoms resulting from lumbar disc herniation: effect on treatment outcomes: analysis of the spine patient outcomes research trial (SPORT). *J Bone Joint Surg Am*. 2011;*93*(20):1906-1914.
9. Carragee EJ, Spinnickie AO, Alamin TF, Paragioudakis S. A prospective controlled study of limited versus subtotal posterior discectomy: short-term outcomes in patients with herniated lumbar intervertebral discs and large posterior anular defect. *Spine*. 2006;*31*(6):653-657.
10. Abdu RW, Abdu WA, Pearson AM, Zhao W, Lurie JD, Weinstein JN. Reoperation for recurrent intervertebral disc herniation in the spine patient outcomes research trial: analysis of rate, risk factors, and outcome. *Spine (Phila Pa 1976)*. 2017;*42*(14):1106-1114.
11. Ledet EH, Jeshuran W, Glennon JC, et al. Small intestinal submucosa for Anular defect closure: long-term response in an: In Vivo: Sheep Model. *Spine*. 2009;*34*(14):1457-1463.
12. Hegewald AA, Medved F, Feng D, et al. Enhancing tissue repair in annulus fibrosus defects of the intervertebral disc: analysis of a bio-integrative annulus implant in an in-vivo ovine model. *J Tissue Eng Regen Med*. 2015;*9*(4):405-414.
13. Hussain I, Sloan SR Jr, Wipplinger C, et al. Mesenchymal stem cell-seeded high-density collagen gel for annular repair: 6-week results from in vivo sheep models. *Neurosurgery*. 2018;*85*(2):E350-E359.
14. Osti OL, Vernon-Roberts B, Fraser RD. Volvo award in experimental studies. Anulus tears and intervertebral disc degeneration. An experimental study using an animal model. *Spine (Phila Pa 1976)*. 1990; *15*(8):762-767.
15. Wei A, Williams LA, Bhargav D, et al. BMP13 prevents the effects of annular injury in an ovine model. *Int J Biol Sci*. 2009;*5*(5):388-396.
16. Melrose J, Shu C, Young C, et al. Mechanical destabilization induced by controlled annular incision of the intervertebral disc Dysregulates metalloproteinase expression and induces disc degeneration. *Spine*. 2012;*37*(1):18-25.
17. Oehme D, Ghosh P, Goldschlager T, et al. Reconstitution of degenerated ovine lumbar discs by STRO-3–positive allogeneic mesenchymal precursor cells combined with pentosan polysulfate. *J Neurosurg Spine SPI*. 2016;*24*(5):715.
18. Shu CC, Dart A, Bell R, et al. Efficacy of administered mesenchymal stem cells in the initiation and co-ordination of repair processes by resident disc cells in an ovine (*Ovis aries*) large destabilizing lesion model of experimental disc degeneration. *Jor Spine*. 2018;*1*(4):e1037.
19. Tsujimoto T, Sudo H, Todoh M, et al. An acellular bioresorbable ultra-purified alginate gel promotes intervertebral disc repair: a preclinical proof-of-concept study. *EBioMedicine*. 2018;*37*:521-534.
20. Oehme D, Ghosh P, Shimmon S, et al. Mesenchymal progenitor cells combined with pentosan polysulfate mediating disc regeneration at the time of microdiscectomy: a preliminary study in an ovine model. *J Neurosurg Spine SPI*. 2014;*20*(6):657.
21. Daly CD, Ghosh P, Zannettino ACW, et al. Mesenchymal progenitor cells primed with pentosan polysulfate promote lumbar intervertebral disc regeneration in an ovine model of microdiscectomy. *Spine J*. 2018;*18*(3):491-506.
22. Reitmaier S, Kreja L, Gruchenberg K, et al. In vivo biofunctional evaluation of hydrogels for disc regeneration. *Eur Spine J*. 2014;*23*(1): 19-26.
23. Grunert P, Hudson KD, Macielak MR, et al. Assessment of intervertebral disc degeneration based on quantitative magnetic resonance imaging analysis: an in vivo study. *Spine*. 2014;*39*(6):E369-E378.
24. Grunert P, Borde BH, Towne SB, et al. Riboflavin crosslinked high-density collagen gel for the repair of annular defects in intervertebral discs: An in vivo study. *Acta Biomater*. 2015;*26*:215-224.
25. Elliott DM, Yerramalli CS, Beckstein JC, Boxberger JI, Johannessen W, Vresilovic EJ. The effect of relative needle diameter in puncture and sham injection animal models of degeneration. *Spine*. 2008;*33*(6):588-596.
26. Singh K, Masuda K, An HS. Animal models for human disc degeneration. *Spine J*. 2005;*5*(6, Supplement):S267-S279.
27. Huang Y-C, Hu Y, Li Z, Luk KDK. Biomaterials for intervertebral disc regeneration: current status and looming challenges. *J Tissue Eng Regen Med*. 2018;*12*(11):2188-2202.
28. Wilke H-J, Kettler A, Wenger KH, Claes LE. Anatomy of the sheep spine and its comparison to the human spine. *Anat Rec*. 1997;*247*(4): 542-555.
29. Mageed M, Berner D, Jülke H, Hohaus C, Brehm W, Gerlach K. Is sheep lumbar spine a suitable alternative model for human spinal researches? Morphometrical comparison study. *Lab Anim Res*. 2013; *29*(4):183-189.
30. Melrose J, Smith SM, Little CB, Moore RJ, Vernon-Roberts B, Fraser RD. Recent advances in annular pathobiology provide insights into rim-lesion mediated intervertebral disc degeneration and potential new approaches to annular repair strategies. *Eur Spine J*. 2008; *17*(9):1131-1148.
31. Alini M, Eisenstein SM, Ito K, et al. Are animal models useful for studying human disc disorders/degeneration? *Eur Spine J*. 2008;*17*(1): 2-19.
32. Sloan SR, Wipplinger C, Kirnaz S, et al. Combined nucleus pulposus augmentation and annulus fibrosus repair prevents acute intervertebral disc degeneration after discectomy. *Sci Transl Med* 2020;*12* (534):eaay2380. https://www.science.org/doi/full/10.1126/scitranslmed.aay2380?casa_token=qo4-TNSUYXcAAAAA%3AMSzsMnteFKUmPhTzHE3r6CPW4swFPoRS50Fuca6WmDHuPi0-qLn9xwbh_bRdMO84ZG9XmKU7aZNG0MLY
33. Pennicooke B, Hussain I, Berlin C, et al. Annulus Fibrosus repair using high-density collagen gel: An in vivo ovine model. *Spine*. 2018;*43*(4): E208-E215.
34. Melrose J, Ghosh P, Taylor TK, et al. A longitudinal study of the matrix changes induced in the intervertebral disc by surgical damage to the annulus fibrosus. *J Orthop Res*. 1992;*10*(5):665-676.
35. Melrose J, Ghosh P, Taylor TK, Vernon-Roberts B, Latham J, Moore R. Elevated synthesis of biglycan and decorin in an ovine annular lesion model of experimental disc degeneration. *Eur Spine J*. 1997;*6*(6):376-384.
36. Melrose J, Smith S, Little CB, Kitson J, Hwa SY, Ghosh P. Spatial and temporal localization of transforming growth factor-beta, fibroblast growth factor-2, and osteonectin, and identification of cells expressing alpha-smooth muscle Actin in the injured anulus fibrosus: implications for extracellular matrix repair. *Spine (Phila Pa 1976)*. 2002;*27*(16):1756-1764.

37. Fardon DF, Milette PC. Nomenclature and classification of lumbar disc pathology. Recommendations of the Combined task Forces of the North American Spine Society, American Society of Spine Radiology, and American Society of Neuroradiology. *Spine (Phila Pa 1976)*. 2001;*26*(5):E93-e113.
38. Pfirrmann CW, Metzdorf A, Zanetti M, Hodler J, Boos N. Magnetic resonance classification of lumbar intervertebral disc degeneration. *Spine (Phila Pa 1976)*. 2001;*26*(17):1873-1878.
39. Shu CC, Smith MM, Smith SM, Dart AJ, Little CB, Melrose J. A Histopathological scheme for the quantitative scoring of intervertebral disc degeneration and the therapeutic utility of adult Mesenchymal stem cells for intervertebral disc regeneration. *Int J Mol Sci*. 2017;*18*(5):1049.
40. Cohen J. A coefficient of agreement for nominal scales. *Educ Psychol Meas*. 1960;*20*(1):37-46.
41. Landis JR, Koch GG. The measurement of observer agreement for categorical data. *Biometrics*. 1977;*33*:159-174.
42. Lotz JC. Animal models of intervertebral disc degeneration: lessons learned. *Spine (Phila Pa 1976)*. 2004;*29*(23):2742-2750.
43. Ghosh P, Moore R, Vernon-Roberts B, et al. Immunoselected STRO-3+ mesenchymal precursor cells and restoration of the extracellular matrix of degenerate intervertebral discs. *J Neurosurg Spine*. 2012;*16*(5):479-488.
44. Iatridis JC, Mente PL, Stokes IA, Aronsson DD, Alini M. Compression-induced changes in intervertebral disc properties in a rat tail model. *Spine (Phila Pa 1976)*. 1999;*24*(10):996-1002.
45. Daly C, Ghosh P, Jenkin G, Oehme D, Goldschlager T. A review of animal models of intervertebral disc degeneration: pathophysiology, regeneration, and translation to the clinic. *Biomed Res Int*. 2016;*2016*:5952165.
46. Klassen PD, Hsu WK, Martens F, et al. Post-lumbar discectomy reoperations that are associated with poor clinical and socioeconomic outcomes can be reduced through use of a novel annular closure device: results from a 2-year randomized controlled trial. *Clinicoecon Outcomes Res*. 2018;*10*:349-357.
47. Oehme D, Ghosh P, Goldschlager T, et al. Radiological, morphological, histological and biochemical changes of lumbar discs in an animal model of disc degeneration suitable for evaluating the potential regenerative capacity of novel biological agents. *J Tiss Sci Eng*. 2015;*6*(2):1.
48. Ahlgren BD, Lui W, Herkowitz HN, Panjabi MM, Tech GJ-P. Effect of Anular repair on the healing strength of the intervertebral disc: a sheep model. *Spine*. 2000;*25*(17):2165-2170.
49. Fuller ES, Shu C, Smith MM, Little CB, Melrose J. Hyaluronan oligosaccharides stimulate matrix metalloproteinase and anabolic gene expression in vitro by intervertebral disc cells and annular repair in vivo. *J Tissue Eng Regen Med*. 2018;*12*(1):e216-e226.
50. McGirt MJ, Eustacchio S, Varga P, et al. A prospective cohort study of close interval computed tomography and magnetic resonance imaging after primary lumbar discectomy: factors associated with recurrent disc herniation and disc height loss. *Spine*. 2009;*34*(19):2044-2051.
51. Brinckmann P, Grootenboer H. Change of disc height, radial disc bulge, and intradiscal pressure from discectomy. An in vitro investigation on human lumbar discs. *Spine*. 1991;*16*(6):641-646.
52. Lebow RL, Adogwa O, Parker SL, Sharma A, Cheng J, McGirt MJ. Asymptomatic same-site recurrent disc herniation after lumbar discectomy: results of a prospective longitudinal study with 2-year serial imaging. *Spine (Phila Pa 1976)*. 2011;*36*(25):2147-2151.
53. Carragee EJ, Han MY, Suen PW, Kim D. Clinical outcomes after lumbar discectomy for sciatica: the effects of fragment type and anular competence. *J Bone Joint Surg Am*. 2003;*85*(1):102-108.
54. Wilke HJ, Kettler A, Claes LE. Are sheep spines a valid biomechanical model for human spines? *Spine (Phila Pa 1976)*. 1997;*22*(20):2365-2374.
55. Gold GE, Han E, Stainsby J, Wright G, Brittain J, Beaulieu C. Musculoskeletal MRI at 3.0 T: relaxation times and image contrast. *AJR Am J Roentgenol*. 2004;*183*(2):343-351.
56. Griffith JF, Wang YX, Antonio GE, et al. Modified Pfirrmann grading system for lumbar intervertebral disc degeneration. *Spine (Phila Pa 1976)*. 2007;*32*(24):E708-E712.
57. Grunert P, Borde BH, Hudson KD, Macielak MR, Bonassar LJ, Härtl R. Annular repair using high-density collagen gel: a rat-tail in vivo model. *Spine*. 2014;*39*(3):198-206.
58. Yuan M, Leong KW, Chan BP. Three-dimensional culture of rabbit nucleus pulposus cells in collagen microspheres. *Spine J*. 2011;*11*(10):947-960.
59. Moliterno JA, Knopman J, Parikh K, et al. Results and risk factors for recurrence following single-level tubular lumbar microdiscectomy. *J Neurosurg Spine*. 2010;*12*(6):680-686.
60. Martin BI, Mirza SK, Flum DR, et al. Repeat surgery after lumbar decompression for herniated disc: the quality implications of hospital and surgeon variation. *Spine J*. 2012;*12*(2):89-97.
61. Ahlgren BD, Vasavada A, Brower RS, Lydon C, Herkowitz HN, Panjabi MM. Anular incision technique on the strength and multidirectional flexibility of the healing intervertebral disc. *Spine (Phila Pa 1976)*. 1994;*19*(8):948-954.
62. O'Connell GD, Vresilovic EJ, Elliott DM. Comparison of animals used in disc research to human lumbar disc geometry. *Spine*. 2007;*32*(3):328-333.
63. Kauppila LI. Ingrowth of blood vessels in disc degeneration. Angiographic and histological studies of cadaveric spines. *J Bone Joint Surg Am*. 1995;*77*(1):26-31.
64. Torre OM, Mroz V, Bartelstein MK, Huang AH, Iatridis JC. Annulus fibrosus cell phenotypes in homeostasis and injury: implications for regenerative strategies. *Ann N Y Acad Sci*. 2019;*1442*(1):61-78.
65. Bogduk N. The lumbar disc and low back pain. *Neurosurg Clin N Am*. 1991;*2*(4):791-806.
66. Shapiro IM, Risbud MV. Introduction to the structure, function, and comparative anatomy of the vertebrae and the intervertebral disc. *The Intervertebral Disc*. Springer; 2014:3-15.
67. Fagan A, Moore R, Vernon Roberts B, Blumbergs P, Fraser R. ISSLS prize winner: the innervation of the intervertebral disc: a quantitative analysis. *Spine (Phila Pa 1976)*. 2003;*28*(23):2570-2576.
68. Freemont AJ, Peacock TE, Goupille P, Hoyland JA, O'Brien J, Jayson MI. Nerve ingrowth into diseased intervertebral disc in chronic back pain. *Lancet*. 1997;*350*(9072):178-181.

SUPPORTING INFORMATION

Additional supporting information may be found in the online version of the article at the publisher's website.

How to cite this article: Constant, C., Hom, W. W., Nehrbass, D., Carmel, E.-N., Albers, C. E., Deml, M. C., Gehweiler, D., Lee, Y., Hecht, A., Grad, S., Iatridis, J. C., & Zeiter, S. (2022). Comparison and optimization of sheep in vivo intervertebral disc injury model. *JOR Spine*, *5*(2), e1198. https://doi.org/10.1002/jsp2.1198